

Effect of matrix thermal properties on laser-induced plasma

Yuheng Shan(单宇恒), An Li(李安), Xinyu Zhang(张新宇), Wen Yi(易文), Ying Zhang(张颖), Xiaodong Liu(刘晓东), and Ruibin Liu(刘瑞斌)

Citation: Chin. Phys. B, 2024, 33 (**10**): 105202. DOI: 10.1088/1674-1056/ad6251
Journal homepage: http://cpb.iphy.ac.cn; http://iopscience.iop.org/cpb

What follows is a list of articles you may be interested in

Transmission effects of high energy nanosecond lasers in laser-induced air plasma under different pressures

Wei-Min Hu(胡蔚敏), Kai-Xin Yin(尹凯欣), Xiao-Jun Wang(王小军), Jing Yang(杨晶), Ke Liu(刘可), Qin-Jun Peng(彭钦军), and Zu-Yan Xu(许祖彦)
Chin. Phys. B, 2023, 32 (**10**): 105201. DOI: 10.1088/1674-1056/acb0bf

Theoretical analyses on the one-dimensional charged particle transport in a decaying plasma under an electrostatic field

Yao-Ting Wang(汪耀庭), Xin-Li Sun(孙鑫礼), Lan-Yue Luo(罗岚月), Zi-Ming Zhang(张子明), He-Ping Li(李和平), Dong-Jun Jiang(姜东君), and Ming-Sheng Zhou(周明胜)
Chin. Phys. B, 2023, 32 (**9**): 095201. DOI: 10.1088/1674-1056/ace033

Combination of spark discharge and nanoparticle-enhanced laser-induced plasma spectroscopy

Qing-Xue Li(李庆雪), Dan Zhang(张丹), Yuan-Fei Jiang(姜远飞), Su-Yu Li(李苏宇), An-Min Chen(陈安民), and Ming-Xing Jin(金明星)
Chin. Phys. B, 2022, 31 (**8**): 085201. DOI: 10.1088/1674-1056/ac597a

Damage characteristics of laser plasma shock wave on rear surface of fused silica glass

Xiong Shen(沈雄), Guo-Ying Feng(冯国英), Sheng Jing(景晟), Jing-Hua Han(韩敬华), Ya-Guo Li(李亚国), Kai Liu(刘锴)
Chin. Phys. B, 2019, 28 (**8**): 085202. DOI: 10.1088/1674-1056/28/8/085202

Conditions for laser-induced plasma to effectively remove nano-particles on silicon surfaces

Jinghua Han(韩敬华), Li Luo(罗莉), Yubo Zhang(张玉波), Ruifeng Hu(胡锐峰), Guoying Feng(冯国英)
Chin. Phys. B, 2016, 25 (**9**): 095204. DOI: 10.1088/1674-1056/25/9/095204

Effect of matrix thermal properties on laser-induced plasma

Yuheng Shan(单宇恒), An Li(李安), Xinyu Zhang(张新宇), Wen Yi(易文),
Ying Zhang(张颖), Xiaodong Liu(刘晓东), and Ruibin Liu(刘瑞斌)†

Key Laboratory of Precision Spectroscopy and Optoelectronic Technology, School of Physics, Beijing Institute of Technology, Beijing 100081, *China*

(Received 8 May 2024; revised manuscript received 19 June 2024; accepted manuscript online 12 July 2024)

The matrix thermal properties have an important impact on laser-induced plasma, as the thermal effect dominates the interaction between ns-pulsed laser and matter, especially in metals. We used a series of pure metals and aluminum alloys to measure plasma temperature and electron density through laser-induced breakdown spectroscopy, in order to investigate the effect of matrix thermal properties on laser-induced plasma. In pure metals, a significant negative linear correlation was observed between the matrix thermal storage coefficient and plasma temperature, while a weak correlation was observed with electron density. The results indicate that metals with low thermal conductivity or specific heat capacity require less laser energy for thermal diffusion or melting and evaporation, resulting in higher ablation rates and higher plasma temperatures. However, considering ionization energy, thermal effects may be a secondary factor affecting electron density. The experiment of aluminum alloy further confirms the influence of thermal conductivity on plasma temperature and its mechanism explanation.

Keywords: laser-induced plasma, thermal properties, matrix effect, thermal storage coefficient, plasma temperature

PACS: 52.38.–r **DOI:** 10.1088/1674-1056/ad6251

1. Introduction

Laser-induced plasma has exotic and complex conditions, ranging in temperature, density, pressure, magnetic field, and electric field.[1] As a spectroscopic diagnostic method based on laser-induced plasma, the laser-induced breakdown spectroscopy (LIBS) technology has been widely used in various fields, such as metallurgy,[2,3] coal industry,[4] environment,[5] and energetic materials,[6] due to its unique advantages of rapid analysis time and little sample damage. However, the matrix effect reduces the accuracy of LIBS. Therefore, it is crucial to understand the correlation between the matrix physical properties and laser-induced plasma. For example, Sattar *et al.*[7] investigated the effect of hardness on the temperature and electron density of laser-induced plasma based on tungsten heavy alloys. The influence mechanism of ablation rate and laser-induced plasma was discussed from the perspectives of grain size and band gap. A surface hardness detecting method based on LIBS for alloys has been proposed. The thermal properties are particularly important in matrix effects, as the thermal effect play a dominant role in the entire process of interaction between ns-pulsed laser and matter. In other words, laser energy promotes the ionization process through thermal conduction. Many studies on the thermal properties of matrix effects focus on matrix temperature or the thermal properties of ambient gases. For example, Liu *et al.*[8] studied the effect of matrix temperature on fs-LIBS signals using a set of copper samples. The results indicate that the increase in sample temperature enhances the emission intensity. High temperature samples have higher plasma temperature and lower electron density. Yu *et al.*[9] used a series of gas mixtures composed of He, Ne, and Ar as the atmosphere for LIBS measurement of titanium alloy samples. The results indicated that changes in gas species mainly affect signal intensity, relative standard deviation, and total number density, rather than plasma temperature and electron density. A preliminary explanation was provided from the aspects of molecular weight, ionization energy, and thermal conductivity of the gas. Salloom *et al.*[10] discussed the correlation between the hardness of Ni–Cr–Nb alloy samples and the spectral line intensity ratio of LIBS spectra, plasma temperature, and electron density. Meanwhile, a semi-empirical formula between plasma temperature and thermal diffusivity was established based only on four samples.

In this paper, we focus on the effect of matrix thermal properties on ns-pulsed LIBS by using a series of pure metals and aluminum alloys. We compared the Saha–Boltzmann plot method and the Boltzmann plot method to calculate the appropriate plasma temperature. Considering the comprehensive effects of thermal conductivity, specific heat capacity, and density, a good correlation between the heat storage coefficient of pure metals and plasma temperature was obtained, and its related mechanism was explained. Considering ionization energy, the effect of thermal properties on electron density was discussed. Finally, the above conclusion and internal mechanism were confirmed and detailed by observing the plasma temperature changes of a group of aluminum alloys with only different thermal conductivities.

†Corresponding author. E-mail: lirsir@bit.edu.cn

© 2024 Chinese Physical Society and IOP Publishing Ltd

2. Experimental

In experiments, 8 different varieties of pure metals (>99% in weight) and 5 different varieties of 5000 series aluminum alloys with standard certificates provided by Jinan Zhongbiao Company were labeled as S1–S8 and A1–A5, respectively. Some important physical properties[11] of all samples are listed in Table 1, and their appearance is shown in Fig. 1(a).

LIBS measurements were conducted using a self-made setup in Fig. 1(a). A Q-switched Nd: YAG laser (Newwave, USA) at 1064 nm with a pulse duration of 3 ns–5 ns and a repetition rate of 1 Hz–10 Hz is utilized as the ablation source. After getting reflected by the mirror (R), the laser pulse was focused on the surface of sample by the lens (L1, $f = 50$ mm) with a spot diameter of approximately 80 μm, and generates a tremendous laser power density over 100 GW·cm^{-2}. After laser ablation, the emission spectra including the plasma continuum radiation and elemental atomic and ionic lines were acquired using a lateral signal collection module, which is composed of two lenses (L2, $f = 50$ mm, L3, $f = 75$ mm) and a fiber ($d = 200$ μm). The spectra were then analyzed using an optical fiber spectrometer. The gate of the spectrometer is controlled by a digital pulse delay generator (DG535, Stanford, USA) with the Q switch signal of laser pulse using as an external trigger source.

For samples S1–S8, a four-channel spectrometer (regions from 180 nm to 690 nm, spectral resolution 0.1 nm, Avantes Avsdesktop USB2, Netherlands) installed with a COMS detector (2048×2048 pixels) was used for spectra collection. The laser energy and integration time were optimized at 24 mJ and 30 μs, respectively. The time delay of 1 μs from the laser light to the spectrometer starting the spectrum collection is optimized.

For samples A1–A5, a four-channel spectrometer (regions from 181 nm to 655 nm, spectral resolution 0.07 nm, Avantes Avsdesktop USB3, Netherlands) was used. The laser energy, integration time and delay time were at 16 mJ, 30 μs, and 1 μs, respectively.

Spectra were collected from 10 repeated pulses at 25 selected positions on the surface of each sample. To reduce the impact of surface differences, such as oxide layer on surface, 5 ablation pulses were performed as pre-pulse at each of the 25 selected points before spectral collection. And as the result, any lines of oxygen were not observed in the collected spectra. Finally, a total of 250 sets of spectral data were collected from each sample.

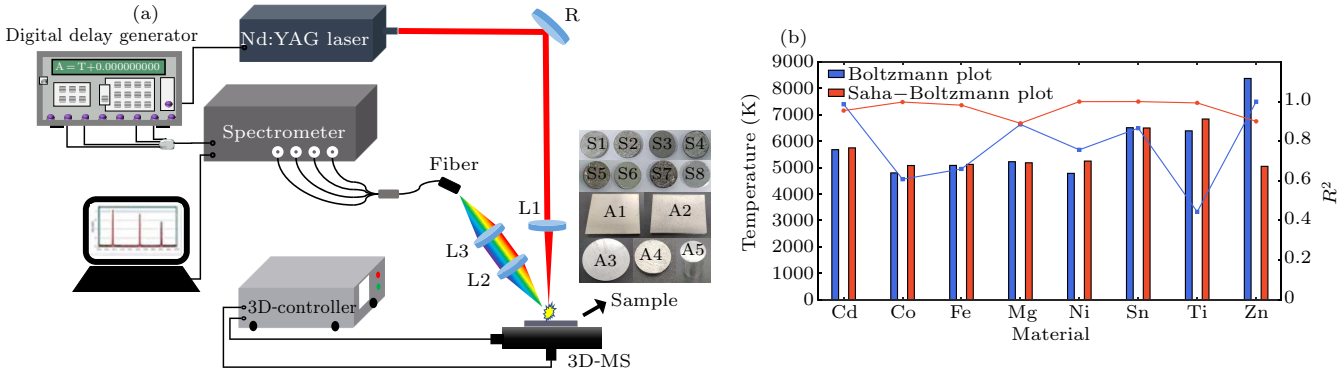


Fig. 1. (a) Schematic diagram of the LIBS setup (R: reflector; L1, L2, L3: lenses 1, 2, 3). (b) Plasma temperature (bars) and corresponding R^2 (lines) of S1–S8 in Boltzmann plot and Saha–Boltzmann plot.

Table 1. The physical properties of the samples (at room temperature).

No.	Name	Density (g/cm^3)	Thermal conductivity (W/(m·K))	Specific heat capacity (J/g·K)	First ionization energy (kJ/mol)	Ablation volume (μm^3)
S1	Cd	8.64	92.0	0.230	867.660	1416
S2	Co	8.80	69.21	0.440	760.304	346
S3	Fe	7.87	76.2	0.440	762.374	394
S4	Mg	1.74	159	1.025	737.654	1667
S5	Ni	8.88	60.7	0.460	737.041	266
S6	Sn	7.29	63.2	0.213	708.489	4080
S7	Ti	4.50	17.0	0.528	658.728	4938
S8	Zn	7.10	112.2	0.3898	906.285	418
A1	aluminum 5005	2.7	200	0.9	–	
A2	aluminum 5050	2.69	193	0.9	–	
A3	aluminum 5052	2.68	138	0.88	–	
A4	aluminum 5154	2.68	125	0.9	–	
A5	aluminum 5083	2.66	117	0.9	–	

The ablation volumes are calculated by measuring the post-ablation surface contours through a step profile, with the results presented in Table 1.

3. Result and discussion

3.1. Laser-induced plasma of pure metals

In laser-induced plasma, the Stark broadening caused by electron radiation dominates the spectral line broadening. The electron density is related to Stark broadening, so it can be estimated by

$$\Delta\lambda_{1/2} = 2\times10^{-22} w n_{\mathrm{e}}, \tag{1}$$

where n_{e} is the electron density, $\Delta\lambda_{1/2}$ is the full width at half maximum of spectral line, and w is the electron collision parameter.[12]

When the plasma satisfies the condition of local thermodynamic equilibrium, the particles on the energy level obey the Boltzmann distribution law. The spectral line intensity is related to the emissivity between energy levels. The plasma temperature can be estimated using Boltzmann plot of atomic spectral lines, as shown below:

$$\ln\frac{\lambda I_\lambda}{g_k A_{ki}} = -\frac{1}{k_{\mathrm{B}}T}E_k + c, \tag{2}$$

where T is the plasma temperature, λ is the wavelength of the line, I_λ is the intensity of spectral line, g_k is the statistical weight for the upper energy level, A_{ki} is the transition probability, k_{B} is the Boltzmann constant, and E_k is the energy of the upper energy level.[13]

The plasma temperature can also be estimated using Saha–Boltzmann plot of both atomic and ionic spectral lines, as shown below:

$$\left(\ln\frac{\lambda I_\lambda}{g_k A_{ki}}\right)^{\wedge} = -\frac{1}{k_{\mathrm{B}}T}E_k^{\wedge} + c. \tag{3}$$

Unlike atomic spectral lines, ionic spectral lines need to be corrected using

$$\left(\ln\frac{\lambda I_\lambda}{g_k A_{ki}}\right)^{\wedge} = \ln\frac{\lambda I_\lambda}{g_k A_{ki}} - \ln\left[2\left(\frac{2\pi m k_{\mathrm{B}}}{h^2}\right)^{3/2}\frac{T^{3/2}}{n_{\mathrm{e}}}\right], \tag{4}$$

$$E_k^{\wedge} = E_k + E_{\mathrm{IP}} + \Delta E, \tag{5}$$

where m is the electron mass, h is the Planck constant, E_{IP} is the ionization energy of element and ΔE is the corresponding plasma interaction correction of ionization energy.[14] Herein, the electronic density n_{e} is calculated through Hα 656.28 nm using Stark broadening method. The atomic and ionic spectral lines used in Boltzmann method and Saha–Boltzmann method, as well as their spectroscopic data A_{ki}, g_k, E_k, E_{IP}, and ΔE were all retrieved from the spectra database of the National Institute of Standards and Technology (NIST).[15]

As shown in Fig. 1(b), the plasma temperatures of pure metals were calculated using Boltzmann plot method and Saha–Boltzmann plot method, as well as the R^2 of the corresponding linear fitting results. The plasma temperatures calculated by the two methods are different, but Saha–Boltzmann plot method shows better performance in fitting. For samples S1–S8, compared to Boltzmann plot method, Saha–Boltzmann plot method usually has a higher R^2 maintained above 0.9. Due to the simultaneous utilization of atomic and ionic spectral lines of the same element, Saha–Boltzmann plot method achieves a wider range of upper energy levels, thereby improving the accuracy of temperature measurement. Therefore, the plasma temperature calculated by Saha–Boltzmann plot method was chosen for subsequent analyses of pure metal samples.

The temperature of the material increases rapidly in the process of continuous absorption of laser energy. The distribution of temperature with time at different depths satisfies

$$\frac{\partial}{\partial t}T(x,t) = \frac{\partial}{\partial x}\left[\left(\frac{\kappa}{C_{\mathrm{p}}\rho}\right)\frac{\partial}{\partial t}T(x,t)\right] + \frac{\alpha}{C_{\mathrm{p}}\rho}I(x,t), \tag{6}$$

where T is the temperature, x is the depth from the surface, κ is the thermal conductivity, C_{p} is the heat capacity, ρ is the density, α is the absorption coefficient, and I is the internal heat source.[16]

In the interaction between laser and material, thermal conductivity, specific heat capacity, and density jointly affect the thermal diffusion on the material surface, thereby affecting the role of laser energy in the core reaction zone, and reflected in the laser-induced plasma. Figures 2(a), 2(b), and 2(c) respectively show the direct relation between laser-induced plasma temperature and the matrix thermal conductivity, specific heat capacity, and density of eight pure metal samples. No significant correlation was observed as the maximum R^2 was less than 0.4. Due to the insufficient number of samples, the simultaneous differences in various matrix properties hide this correlation. Considering that the loss of laser energy is not limited to thermal diffusion, and the energy remaining on the local surface has a more significant impact on the plasma temperature. Herein, the thermal storage coefficient S is introduced, which can characterize the ability of materials to store heat in local areas, involving the thermal conductivity, heat capacity, and density of the matrix, as shown below:

$$S = \sqrt{\frac{2\pi\rho C_{\mathrm{p}}\kappa}{\tau}}, \tag{7}$$

where τ is the harmonic period, usually taken as 24 hours.[17]

Figure 2(d) shows the variation of the laser-induced plasma temperature with the heat storage coefficient. It can be considered that the laser-induced plasma temperature has a negative linear correlation with the heat storage coefficient of the matrix, as R^2 is greater than 0.95. This means that the plasma temperature is negatively correlated with the thermal

conductivity, specific heat capacity, and density of the matrix. When the ns-pulsed laser is focused on the surface of the sample, metal materials with lower thermal conductivity dissipate less energy through thermal diffusion. Then, larger laser energy deposits in smaller local areas, leading to increased ablation. For materials with lower specific heat capacity and density, melting and vaporization within a local range on the surface require less laser energy. Therefore, it will lead to higher ablation efficiency and faster temperature rise. Considering the above points, there is less laser energy used for thermal diffusion or melting and vaporization for metal materials with low heat storage coefficients. So, more laser energy can be absorbed by subsequent laser-induced plasma, ultimately leading to a higher temperature of laser-induced plasma.

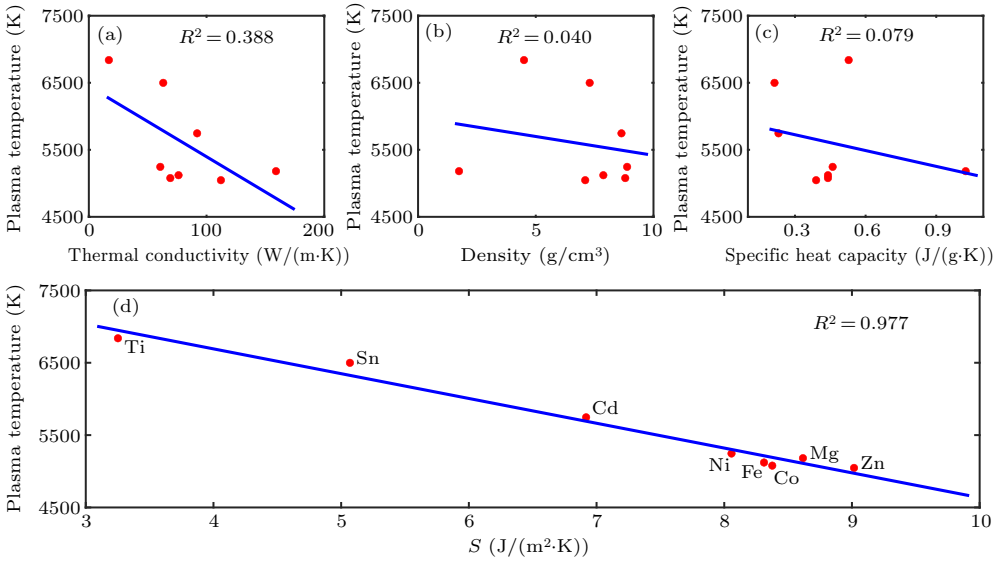


Fig. 2. Correlation between the laser-induced plasma temperature and the matrix (a) thermal conductivity, (b) density, (c) specific heat capacity, (d) heat storage coefficient of pure metals.

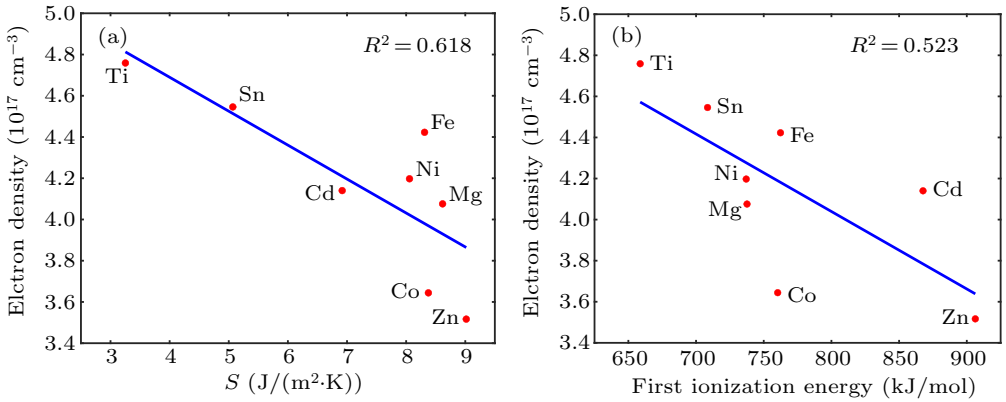


Fig. 3. Correlation between the laser-induced plasma electron density and the matrix (a) heat storage coefficient and (b) first ionization energy of pure metals.

In Fig. 3(a), there is a weak negative correlation between plasma electron density and the heat storage coefficient, with an R^2 of only 0.618. However, this does not invalidate the previous interpretation of the role of thermal properties in the LIBS matrix effect. In addition to the thermal effect of laser energy in the matrix, another important factor to be considered is the ionization energy of matrix elements. The electron density depends on the absorption of laser energy by the plasma, while ionization energy greatly affects the plasma shielding effect.[18] The secondary or higher ionization inside the plasma is much lower than that of first ionization and can be ignored to some extent, so the first ionization energy should be significantly correlated with the electron density of laser induced plasma. However, the negative correlation between electron density and the first ionization energy is also at a relatively low level, as shown in Fig. 3(b), where R^2 is only 0.523. The low heat storage coefficient increases plasma electron density by the enhancement of the ablation rate and mass, but the combined effect with other matrix parameters (such as the first ionization energy) weakens the direct manifestation of this correlation when the sample size is insufficient. These indicate that the influence of laser absorption or shielding on plasma electron density takes into account the contribution of more parameters, while thermal properties may be a secondary

factor. A more comprehensive and accurate model needs to be established to explain the impact of various matrix parameters, including thermal properties, on the complex evolution process of plasma.

3.2. Laser-induced plasma of aluminum alloys

Samples A1–A5 were used for further discussion and confirmation of the correlation between the thermal conductivity of the matrix and the laser-induced plasma. Taking sample A1 as a representative, figure 4(a) shows the typical LIBS spectrum of this type of aluminum magnesium alloy. The determination of spectral lines was based on the NIST spectral database.[15] As shown in Table 1, 5 different 5000 series aluminum alloys have similar densities and specific heat capacities, but differ greatly in thermal conductivity, highlighting the effect of metal thermal conductivity on laser-induced plasma. Herein, the Boltzmann plot method was used to evaluate the plasma temperature based on Al atomic spectral lines, as all fits in A1–A5 already have R^2 exceeding 0.93.

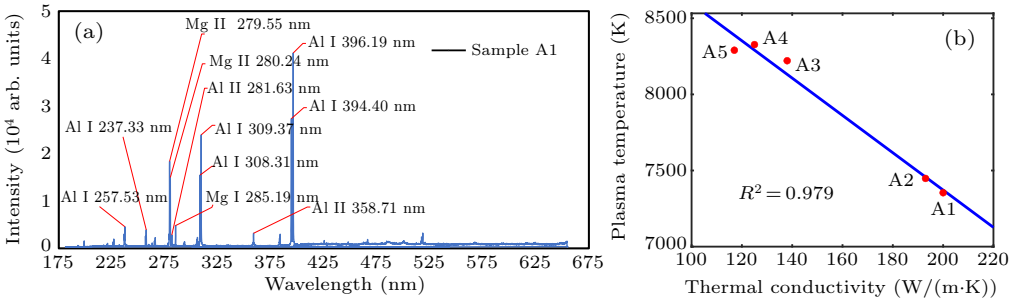


Fig. 4. (a) The spectra of sample A1. (b) Correlation between the laser-induced plasma temperature and the matrix thermal conductivity of aluminum alloys.

Figure 4(b) shows a negative linear correlation between the laser-induced plasma temperature and the thermal conductivity of aluminum alloys, with an R^2 of 0.979, which is consistent with the interpretation of the thermal conductivity obtained in laser-induced plasma of pure metals. In metal materials, the energy transfer between free electrons plays the major role in thermal conduction. In the temperature field, high temperature electrons will move rapidly and exchange energy with low temperature electrons through collisions.[19]

As shown in Eq. (6), when the heat capacity, mass density, and absorption coefficient are similar, materials with lower thermal conductivity dissipate less energy during thermal conduction, which means that the energy transferred to new free electrons through collisions will be reduced. At the same time, more laser pulse energy will be accumulated in the small local areas on the surface and be absorbed by free electrons, resulting in smaller ablation range and higher energy density. In this way, more energy is absorbed by fewer free electrons and electrons obtain greater kinetic energy. Therefore, more materials are more likely to reach the plasma state generated by melting and vaporization. The initial temperature and ionization degree of the plasma generated during this process are relatively high, ultimately leading to a higher plasma temperature.

4. Conclusion and perspectives

In conclusion, we used a group of samples, including pure metals and aluminum alloys, to investigate the effect of matrix thermal properties on ns-pulsed laser-induced plasma. The plasma temperature and electron density were determined by spectroscopy and were correlated with the matrix properties, including thermal conductivity, specific heat capacity, density, and first ionization energy. In the pure metal experiment, heat storage coefficients calculated from thermal conductivity, heat capacity, and density were introduced, and a significant negative correlation was observed with plasma temperature. These observations are explainable considering that metal materials with low thermal conductivity and low specific heat capacity require less laser energy for thermal diffusion or melting and vaporization, resulting in higher ablation rates and higher plasma temperatures. The weak negative correlation between plasma electron density and heat storage coefficient leads to an interpretation that thermal properties play a secondary role in the matrix effect of laser absorption or shielding on plasma electron density. In the experiment of aluminum alloys, the direct correlation between thermal conductivity and plasma temperature provides a more detailed discussion, strongly confirming the conclusion of thermal effects in pure metals. Overall, this also reveals the impact of thermal effects on LIBS spectral acquisition and is expected to provide a new approach for measuring the thermal properties of unknown metals.

Acknowledgement

Project supported by the National Key Research and Development Project (Grant No. 2018YFC2001100).

References

[1] Harilal S S, Phillips M C, Froula D H, Anoop K K, Issac R C and Beg F N 2022 *Rev. Mod. Phys.* **94** 035002
[2] Díaz-Romero D, Van den Eynde S, Zaplana I, Zhou C, Sterkens W, Goedemé T and Peeters J 2023 *Resources, Conservation and Recycling* **190** 106865

[3] Li Q X, Zhang D, Jiang Y F, Li S Y, Chen A M and Jin M X 2022 *Chin. Phys. B* **31** 085201
[4] Xu X, Li A, Wang X, Ding C, Qiu S, He Y, Lu T, He F, Zou B and Liu R 2020 *Journal of Analytical Atomic Spectrometry* **35** 984
[5] Zhang Y, Zhang T and Li H 2021 *Spectrochimica Acta Part B: Atomic Spectroscopy* **181** 106218
[6] Li A, Zhang X, Yin Y, Wang X, He Y, Shan Y, Zhang Y, Liu X, Zhong L and Liu R 2023 *Journal of Analytical Atomic Spectrometry* **38** 810
[7] Sattar H, Ran H, Ding W, Imran M, Amir M and Ding H 2019 *Appl. Phys. B* **126** 5
[8] Liu Y, Wang Q, Jiang L, Chen A, Han J and Jin M 2022 *Chin. Phys. B* **31** 105201
[9] Yu J, Hou Z, Ma Y, Li T, Fu Y, Wang Y, Li Z and Wang Z 2020 *Spectrochimica Acta Part B: Atomic Spectroscopy* **174** 105992
[10] Salloom H and Hamad T 2021 *Optica Applicata* **51** B13
[11] Association A 2000 *Aluminum Standards And Data* (Aluminum Standards And Data)
[12] El Sherbini A M, Hegazy H and El Sherbini T M 2006 *Spectrochimica Acta Part B: Atomic Spectroscopy* **61** 532
[13] Bousquet B, Gardette V, Ros V M, Gaudiuso R, Dell'Aglio M and De Giacomo A 2023 *Spectrochimica Acta Part B: Atomic Spectroscopy* **204** 106686
[14] Aguilera J A and Aragón C 2007 *Spectrochimica Acta Part B: Atomic Spectroscopy* **62** 378
[15] Kramida A, Ralchenko Y, Reader J and Team N A 2021 *NIST Atomic Spectra Database*, version 5.9 (Gaithersburg: National Institute of Standards and Technology)
[16] Ho J, Grigoropoulos C and Humphrey J 1995 *J. Appl. Phys.* **78** 4696
[17] Singh R and Dabas M *Defect and Diffusion Forum*, pp. 73–78
[18] Cristoforetti G, Legnaioli S, Palleschi V, Salvetti A and Tognoni E 2008 *Spectrochimica Acta Part B: Atomic Spectroscopy* **63** 312
[19] Li S, Yang X, Hou J and Du W 2020 *Journal of Magnesium and Alloys* **8** 78